JOURNAL OF AIRCRAFT
Vol. 44, No. 2, March–April 2007

Experimental Investigation into the Aerodynamics of Battle Damaged Airfoils

Peter M. Render,* Suraj de Silva,† and Andrew J. Walton†
Loughborough University, Loughborough, Leicestershire LE11 3TU, England, United Kingdom
and
Mani Mahmoud‡
Amirkabir University of Technology, 15875 Tehran, Iran

DOI: 10.2514/1.24144

Wind tunnel tests are reported that investigate three aspects of aerodynamic flows through battle damaged airfoils. The first aspect investigated was the effect of camber. This showed that reducing camber weakened the strength of the jet flow through the damage and delayed the onset of strong jet flows to higher incidences. The second investigation used five hole probe measurements to survey the flow field on a battle damaged flat plate airfoil. The measurements indicated that the use of the jet-to-freestream velocity ratio is a poor criteria for determining whether damage flows have undergone transition to strong jets. Finally, the influence of a star shaped hole to simulate more realistic battle damage was investigated. It was shown that in terms of damage flow characteristics and changes in lift, drag, and pitching moment coefficients, the use of a circular hole is a reasonable simulation of battle damage.

Nomenclature

C_D	=	drag coefficient
C_L	=	lift coefficient
C_M	=	pitching moment coefficient
C_p	=	pressure coefficient
Cp_{us}	=	upper surface static pressure coefficient
c	=	chord
D	=	diameter of hole for jet-in-crossflow studies
dC_D	=	increment of drag coefficient.
dC_L	=	increment of lift coefficient.
dC_M	=	increment of pitching moment coefficient
M_R	=	jet-to-freestream momentum ratio
R	=	jet-to-freestream velocity ratio
r	=	radius of battle damage hole
U_{true}	=	total velocity measured by five hole probe
U_∞	=	freestream velocity of wind tunnel
u	=	velocity component in the x direction
u_m	=	velocity component in the x direction (model axes)
v	=	velocity component in the y direction
v_m	=	velocity component in the y direction (model axes)
w	=	velocity component in the z direction
w_m	=	velocity component in the z direction (model axes)
X	=	distance along chord of flat plate, measured from center of hole
x	=	distance along chord of airfoil, measured from leading edge of the model
Y	=	distance along span of flat plate, measured from center of hole
y	=	distance along the span of the airfoil, measured from model centerline
z	=	distance normal from the upper surface of the airfoil
ΔC_p	=	change in static pressure coefficient

Subscripts

damaged	=	results for model with damage
max	=	maximum
undamaged	=	results for undamaged model

Introduction

VERY little experimental work has been undertaken into the aerodynamic effects of battle damage to wings [1]. Until recently, published work has considered the effects of simple forms of damage on aircraft models at high speeds [2–4], whereas examinations into low-speed characteristics [1,5–8] have failed to explain the underlying flow physics behind the identified aerodynamic effects. This lack of data led to the initiation of battle damage studies at Loughborough University with the first study by Irwin extensively reported [9–12]. Studies into the aerodynamic effects of battle damage have continued, and this paper provides information on the following:

1) The influence of airfoil camber on battle damage aerodynamics.
2) The structure of the air flow through battle damage.
3) The acceptability of using simple circular holes to model battle damage.

This last point is important because battle damage may be random in shape and not easily approximated to the regular circular holes used by Irwin, Robinson [8], and others.

Previous Studies

Irwin conducted a series of wind tunnel experiments to determine how the aerodynamic characteristics of a two-dimensional NACA 64_1–412 airfoil were influenced by the presence of simulated gunfire or missile damage. Using a wind tunnel balance, the increments in drag, lift, and pitching moment coefficients, relative to an undamaged airfoil, were determined for each of the damage cases. To assist in the analysis, balance measurements were supplemented by flow visualization and surface static pressure readings. To allow the use of larger models and more precise damage modeling, the ratio of model chord to tunnel height exceeded the recommended maximum

Received 23 March 2006; revision received 15 August 2006; accepted for publication 15 August 2006.

*Senior Lecturer, Department of Aeronautical and Automotive Engineering. AIAA Senior Member.
†Research Student, Department of Aeronautical and Automotive Engineering.
‡Professor, Aerospace Engineering Department, Somaie Street, Hafez Avenue. AIAA Senior Member.

for wind tunnel correction methods. By testing two different chord sizes (100 and 200 mm) of the undamaged NACA 64_1–412 airfoil at identical Reynolds numbers, Irwin [11] demonstrated that the correction methods remained valid for the larger model.

To keep the number of tests to manageable proportions, it was necessary to reduce the large number of possible damage forms into a small number of representative types. The rationale by which these types were selected is summarized in [11]. Gunfire damage was represented by single circular holes passing through the model, with diameters ranging from 10 to 40% of airfoil chord. Each hole was centered at four different locations on the airfoil, that is, leading edge, quarter chord, half-chord, and trailing edge. It was concluded that increasing hole diameter resulted in greater lift loss and increased drag, and in addition, the quarter and half-chord locations produced the greatest adverse influence on aerodynamic performance. This influence on the aerodynamic coefficients was attributed to air flow through the hole, with the trends in coefficients and behavior of the air flow consistent for both quarter and half-chord locations. The air flow was driven by the pressure differential between the upper and lower wing surfaces, and took one of two forms. The first was a "weak jet" (Fig. 1) that formed an attached wake behind the damage hole. Upstream of the damage, where the surface flow met the jet, a "horseshoe vortex" was formed that wrapped around the damage and the wake. The weak jet gave the smallest changes in force and moment coefficients, and resulted in a limited disruption of the pressure distribution on the surface of the wing. The second form (Fig. 2) resulted from either increased incidence or damage size. This was the "strong jet" where the flow through the hole penetrated into the freestream resulting in extensive separation of the oncoming surface flow, and the development of a separated wake with reverse flow. Compared with the weak jet, the effect on force and moment coefficients was increased, and the influence on the airfoil pressure distribution extended significantly in a spanwise direction.

Irwin carried out his studies on hollow models that represented the twin spar arrangement typical of many aircraft wings. To investigate the influence of internal wing geometry, Irwin also tested some NACA 64_1–412 models of solid construction [10,12]. Using a solid model produced similar trends in the lift and drag effects of simulated gunfire damage, although the solid model produced a greater lift loss and higher drag than the hollow model. These effects became more significant with an increase in incidence and hole diameter.

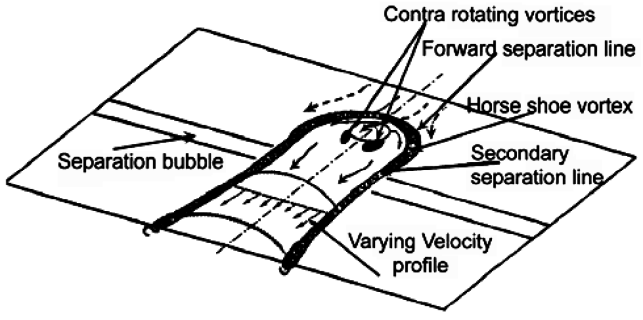

Fig. 1 Weak jet [11].

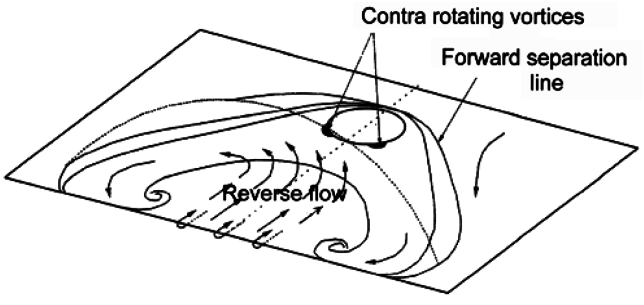

Fig. 2 Strong jet [11].

The findings of Robinson [8], who investigated ballistic effects on helicopter rotor airfoils, are broadly in line with those of Irwin. Robinson tested two different airfoil shapes and concluded that different geometries played only a minor role in the aerodynamic degradation associated with battle damage. Robinson also used serrations to simulate the petalling that often takes place around a hole when a projectile passes through a metal structure. These serrations were $0.024c$ high, but did not substantially affect the damage flow, although the downstream wake tended to be more energetic. In terms of the aerodynamic performance it was concluded that the hole, rather than the serrations, was the dominant source of the degradation.

Rationale Behind the Studies

Irwin's results were for one specific airfoil, but the trends in coefficient increments and the flow mechanisms he identified should be applicable to all lifting surfaces with simulated gunfire damage at any "mid" chord location (i.e., away from the leading and trailing edges). For example, because the influence on aerodynamic coefficients is primarily due to flow through the damage hole, changing airfoil camber will change the differential pressure between upper and lower surfaces and change the resulting aerodynamic force increments. A wind tunnel investigation into the effects of camber was carried out using two NACA airfoils, each of 200 mm chord and identical thickness forms, but with different cambers. Results were obtained for the symmetric NACA 64_1–012 airfoil in the undamaged state and with simulated gunfire damage of 10 to 40% chord located at quarter chord. This allowed direct comparison with the results for the NACA 64_1–412 obtained by Irwin [11].

Although flow visualization and surface pressure measurements have given a good indication of the flow mechanisms involved in battle damage flow, there are currently no published flow field measurements, such as velocity and orientation, in the vicinity of battle damage. An interesting feature of Irwin's work was the identified similarity between the flow fields of battle damage airfoils and "jets in crossflow." This similarity occurred despite fundamental differences between the two kinds of experiments. For example, in the battle damage experiments the jet issued from a curved surface at incidence, whereas most jets-in-crossflow experiments issue from flat plates. To investigate these similarities flow field measurements were carried out on a battle damaged flat plate airfoil. The desire to maintain as much geometric similarity as possible with Irwin's work meant that the flat plate had the same chord (200 mm) and a similar thickness chord ratio (12.5%) as the NACA 64_1–412 airfoil. The flat plate incorporated a 2:1 elliptical leading edge to delay flow separation, whereas the trailing edge was tapered from 70% chord to reduce the wake. Although the tapered trailing edge imparted a degree of camber, the airfoil was nevertheless flat with zero camber over most of its chord, and indeed over the area of interest, where the damage hole would be located. Thus the camber due to the tapered trailing edge was expected to have little influence on the creation of the jet and the surrounding flow field. Therefore, this particular flat plate geometry was an intermediate configuration between thin flat plates normally used in jets-in-crossflow investigations and the NACA airfoil used by Irwin. Locating the damage at quarter chord would have meant that the forward edge of the hole would have been close to the elliptical nose of the flat plate. The basic flow mechanisms identified by Irwin are applicable to all midchord locations. Therefore, the decision was made to locate a $20\%c$ hole at 30% chord. Again based on Irwin's work, this particular diameter was likely to produce both weak and strong jets, while being large enough to enable an adequate spatial resolution for velocity measurements.

A possible criticism that may be leveled at Irwin, and some other battle damage studies, is that they used circular holes to simulate battle damage. In fact, the same criticism can be leveled at two of the studies reported in this paper. Real battle damage may produce holes with jagged edges that may not approximate to circular shapes. Experiments from jets in crossflow have shown that jets from different shaped holes produce different flow characteristics to

circular holes [13]. It is unknown to what extent circular holes are a reasonable approximation to real battle damage, and for that reason an investigation into the influence of hole shape was carried out. The influence of petalling around damage holes was not considered. In real life, studies have shown that petalling is typically less than $0.006c$ [11] and would therefore be difficult to reproduce and accurately measure its effects at model scale. In addition, Robinson [8] with significantly larger serrations ($0.024c$) concluded that the hole was the dominant effect.

The influence of an alternative battle damage shape with sharp corners was investigated using star shaped battle damage on a NACA 64_1–412 airfoil of 200 mm chord. This investigation was part of a larger study into the effects of hole shape, which has been reported by Mahmoud [14]. In this study the centroid of an equilateral triangle was positioned at half-chord with its apex nearest to the leading edge of the airfoil. The area of the triangle equaled a circle of 20% chord diameter, resulting in sides of length 54 mm. The star shaped damage reported here was constructed by machining a second equilateral triangle shape, but rotated through 180 deg to give a symmetric six point star. The center of the resulting star was located at half-chord and had an area corresponding to a circular hole of 23% chord diameter. The choice of half-chord location allowed comparison with one of the cases reported by Irwin [12], from which the results of [11] have been extracted.

All of the models tested were of solid construction. The drag and lift characteristics of the battle damage are compared with Irwin's hollow model data. This comparison is valid, because all of the presented data are for damage holes with an effective diameter of 23%c or less. From Irwin's work, the influence of internal geometry is believed to be small.

Experimental Arrangements

Camber and Noncircular Hole Studies

The tests were carried out using Irwin's experimental arrangement (Fig. 3), and used a 0.45×0.45 m closed working section low turbulence wind tunnel, with a turbulence intensity of better than 0.1%. Full span airfoil models were mounted, via struts, onto a three component balance located beneath the working section of the wind tunnel. Nominal balance accuracy was better than 0.05% full scale deflection for all components. Balance measurements were read via a 16 bit data logging system connected to a personal computer. Wind tunnel corrections were applied using [15].

Unless stated, the models were tested with natural transition, at a Reynolds number of 5×10^5 based on airfoil chord, which corresponds to a freestream velocity of 36 m/s. Each model was tested in both the undamaged and damaged states. Before applying any damage, the results for the undamaged NACA 64_1–412 airfoil were compared with data from Loftin and Smith [16], who tested the same airfoil at a Reynolds number of 7×10^5. Although, compared with the present study, there was a slight mismatch in the Reynolds number, the differences between the two sets of data were consistent with typical Reynolds number effects. In addition, data from the present study showed good agreement with the results of Irwin [11].

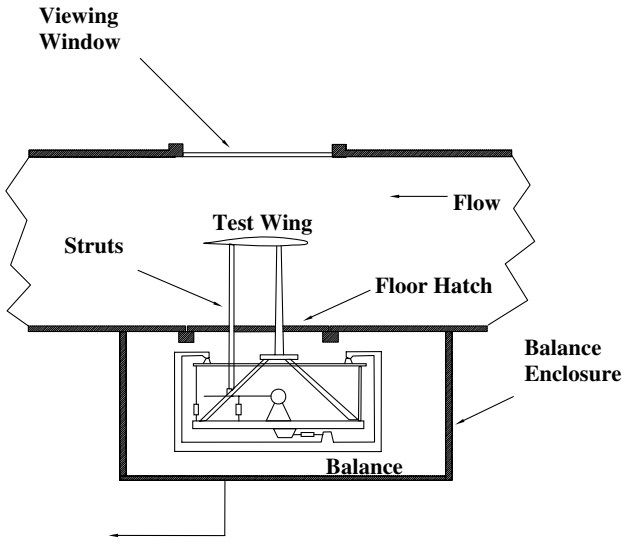

Fig. 3 Experimental arrangement [11].

Damage was applied at mid span of the model. Once the experimental data had been reduced to coefficient form, the influence of the damage was determined in terms of increments given by

$$dC_D = C_{D\,\text{damaged}} - C_{D\,\text{undamaged}} \tag{1}$$

$$dC_L = C_{L\,\text{damaged}} - C_{L\,\text{undamaged}} \tag{2}$$

$$dC_M = C_{M\,\text{damaged}} - C_{M\,\text{undamaged}} \tag{3}$$

where C_D, C_L, and C_M denote drag, lift, and pitching moments, respectively. Assessment of accuracy and repeatability indicated that the uncertainties in the increments were ± 0.015 for lift, ± 0.001 for drag, and ± 0.003 for pitching moment.

Flat Plate Study

The 0.45×0.45 m wind tunnel was again used, but this time the model was mounted so that it spanned the tunnel vertically. This arrangement avoided the need for struts. A turntable in the floor of the working section was used to vary model incidence. The Reynolds number was 5×10^5, although boundary layer transition was forced by carefully wrapping 400 grit wet and dry abrasive sheet around the leading edge from the 10% chord on the upper surface to 15% chord on the lower surface. This was necessary because the airfoil stalled before strong jet conditions were established at the damage, and also ensured that the boundary layer on the lower surface was turbulent before encountering the damage. Flow field velocity measurements were carried out using a miniature five hole pressure probe, where the diameter across the probe head was 1.7 mm. The probe had been previously calibrated over pitch and yaw ranges of ± 36 deg with a nominal accuracy of ± 1 deg. The probe was connected to five Furness FCO44 pressure transducers with a pressure range of ± 100 mm H_2O. The accuracy of these transducers was measured and found to be such that the nominal error was within $\pm 0.2\%$ of reading and a repeatability of $\pm 0.2\%$. The probe was inserted into the working section through the top wall of the wind tunnel and traversed around the flow field using a 3-dimensional traverse mechanism mounted above the wind tunnel. The traverse mechanism allowed measurements in discrete planes perpendicular to the freestream flow direction. Once measurements in a particular plane were completed, the probe was manually moved to the next measurement plane. The nominal accuracies of the traverse mechanism were estimated to be no greater than 0.15 mm ($0.00075c$) along the y and z axes and 1 mm along the x axis. An example of the repeatability for the flow field measurements is illustrated in Table 1, which shows the proportion of measurements falling within certain tolerance bands.

The tolerances shown in Table 1 correspond to the difference in the nondimensional velocity components at the same location between successive measurements, where

Table 1 Repeatability for velocity measurements on the damaged flat plate at 4 deg incidence

Velocity component	Tolerance		
	± 0.1	± 0.05	± 0.02
u_m	100%	99%	96%
v_m	100%	100%	99%
w_m	100%	100%	100%
U_{true}	100%	99%	96%

$$\text{tolerance}\,(u_m) = \left(\frac{u_m}{U_\infty}\right)_{\text{original}} - \left(\frac{u_m}{U_\infty}\right)_{\text{repeatability}} \quad (4)$$

The results presented have not been corrected for tunnel constraints, because at nonzero incidences, the corrections to freestream velocity would vary along the chord of the flat plate. Use of [15] indicated that the correction to freestream velocity typically varied between 1.5% at zero incidence to 3.0% at 12 deg.

Measurement of the surface static pressure field was carried out using five rows each of 47 chordwise pressure tappings around the upper and lower surfaces of the model. The rows were located on the center line of the damage and at $0.5r$, $1.5r$, $2.5r$, and $5.0r$ from the center line, where r was the radius of the damage. The tappings were connected to a Setra 239 pressure transducer (of ± 7.5 in. H_2O range) via a 48D9 Scanivalve. The accuracy of the transducer was 0.1% of full scale reading and repeatability of C_p was shown to be better than ± 0.02.

For all of the studies reported here, surface flow visualization was carried out using a mixture of titanium dioxide and paraffin.

Influence of Camber

Results for the battle damaged symmetric NACA 64_1–012 airfoil were consistent with the trends identified by Irwin for the NACA 64_1–012, namely

1) For most of the incidence range, the flow through the 10% chord damage was a weak jet and produced small increases in C_D (typically less than 0.003) for both positive and negative incidences. Changes in C_L at these incidences were negligible.

2) Drag increments increased with hole size, and up to the onset of stall, increased with incidence.

3) For positive incidences, lift increments became more negative with increased hole size, and up to the onset of stall decreased further with increased incidence. (Note that as the airfoil was symmetric, the increments became positive at negative incidences, that is, the direction of the flow through the damage was reversed).

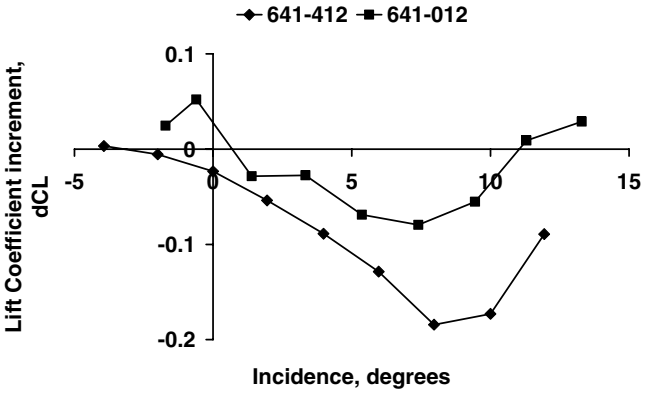

Fig. 4 Influence of camber on lift coefficient increments.

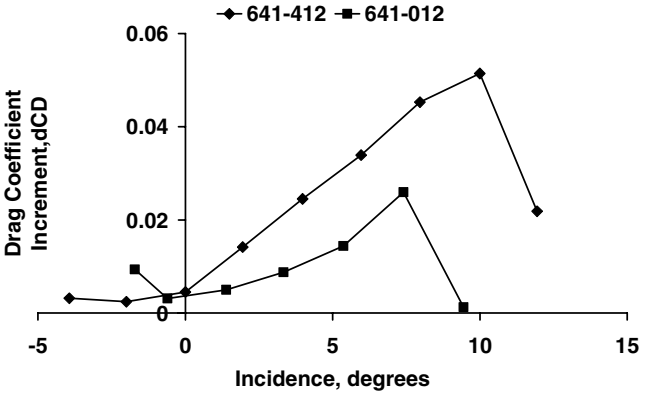

Fig. 5 Influence of camber on drag coefficient increments.

Table 2 Influence of camber on transition from weak to strong jet for a range of damage sizes

Aerofoil	10%c	20%c	30%c	40%c
64_1–012	8–10 deg	6–8 deg	4–6 deg	0–2 deg
64_1–412	6–8 deg	0–2 deg	——	——

Although the trends for the two airfoils were consistent, there were significant differences in the increment values. This is illustrated in Figs. 4 and 5, which are for 20% chord damage. It can be seen that at positive incidences, reducing camber resulted in decreased drag and less negative lift increments. Flow visualization studies showed that for a given incidence, removing camber reduced the extent of the jet flow through the damage, and often changed a strong jet into a weak jet. An alternative way of expressing this effect is to note that reducing camber delayed the weak to strong jet transition to higher incidences, for all damage sizes. This is illustrated by Table 2, which was determined from flow visualization.

For each airfoil-damage combination, at the lower incidence, a weak jet was present, whereas for the higher incidence a strong jet was present. Therefore transition took place between these two values. The flow visualization results (i.e., delayed transition and reduced extent of the flow through the damage) indicate a weakening of the damage jet with reduced camber, which in turn resulted in the improved lift and drag increments shown in Figs. 4 and 5.

Flat Plate Results

Surface Flow Visualization

Figure 6 shows the surface flow visualization for the damaged flat plate model at 12 deg incidence. The flow resembles a strong jet, although it was not exactly similar to that observed by Irwin. The flow here appears to be in transition from weak to strong jet. A key feature of strong jet flow is a large triangular region of reverse flow located toward the trailing edge and between two strong contrarotating vortices. This region can be seen to develop in Fig. 6, where a small triangular region of reverse flow is created near the trailing edge and appears to feed up the center line until almost up to the damage. This reverse flow region is much smaller in area than those observed by Irwin. This suggests that the low structure seen here is intermediate between a weak jet and a strong jet. Also evident are the centers of the two contrarotating vortices along the rear edge of the damage hole. These vortices are wider apart than expected for a weak jet, yet closer than those of a fully developed strong jet. The vortices are displaced slightly away from the edge of the hole. Joining the two vortices is a separation line, which is the boundary between the jet and the previously described reverse flow. At the edge of the hole, on either side and slightly forward of the

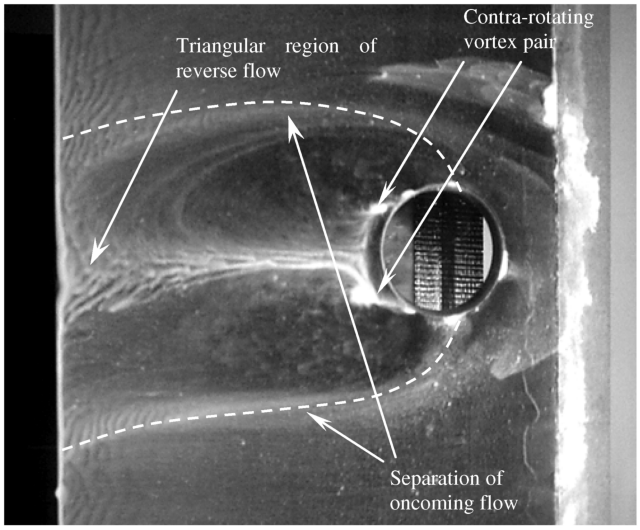

Fig. 6 Flow visualization for damaged flat plate at 12 deg incidence.

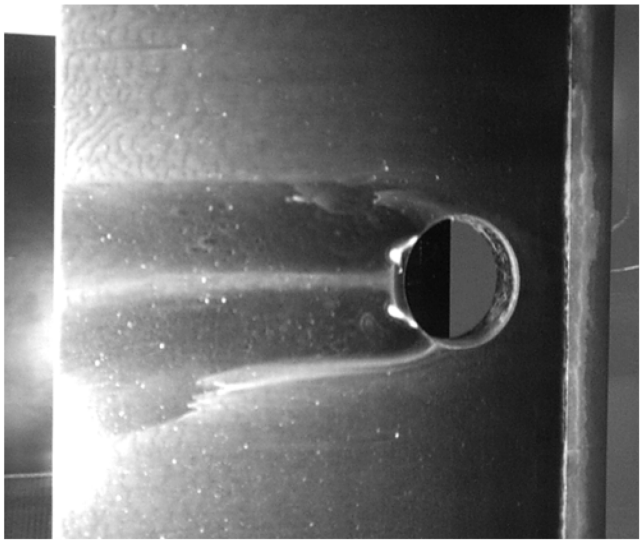

Fig. 7 Flow visualization for damaged flat plate at 8 deg incidence.

contrarotating vortices, is an area where the flow visualization liquid has collected that indicates the forward edge of the jet.

Another key difference between the flow structure shown in Fig. 6 and that of a strong jet is the separation line of the oncoming flow. Separation occurs after the flow has passed the upstream edge of the hole, and not before. This suggests that the jet exits only through the rear portion of the damage hole, rather than completely filling the hole. As the angle of attack was reduced to 8 deg (Fig. 7), the flow structure changed and resembled a weak jet flow. The triangular region of reverse flow is not evident, whereas the contrarotating vortices at the rear edge of the damage hole are closer together. The separation line of the oncoming flow has moved farther back, as the jet exits from an even smaller region of the damage hole. When the angle of attack was further reduced to 4 deg the contrarotating vortex pair and the separation line of the oncoming flow completely disappeared. There was no jet flow through the damage hole and the oncoming flow merely "dipped" in and out of the hole, akin to a cavity flow.

Induced Changes in the Surface Pressure Field due to Through-Hole Jet

Figures 8 and 9 show ΔC_p for the upper surface at two different incidences, where ΔC_p is defined as

$$\Delta C_P = (C_{P_{\mathrm{US}}})_{\mathrm{damaged}} - (C_{P_{\mathrm{US}}})_{\mathrm{undamaged}} \tag{5}$$

and is effectively the induced changes in the static pressure field due to the jet flow through the damage.

Results of jets-in-crossflow studies [17–19] identify three regions, the details of which depend on the ratio of R. These regions can be identified in Fig. 10, which is a representative plot reproduced from [17] and shows the change in pressure coefficient between jet on and jet off. The regions are the following:

1) Positive C_p region forward of the jet resulting from blockage effects on the freestream flow.

2) Negative pressure region located on either side of the jet due to acceleration of the freestream flow.

3) Distorted negative pressure region downstream of the exit due to the proximity of the deflected jet.

At 12 deg the jet flow exiting from the damage induced significant pressure changes on the upper surface, and in Fig. 8 all three of the above regions can be seen. However, their magnitude and precise locations differ. The first region, of positive induced C_p, can be seen ahead of the damage hole. This is consistent with the retardation of the oncoming freestream flow as it approaches the jet, resulting in increased static pressures. The extent of this positive region, however, differs from observations of jets in crossflow, where the positive C_p region is found to end at the forward edge of the hole/jet.

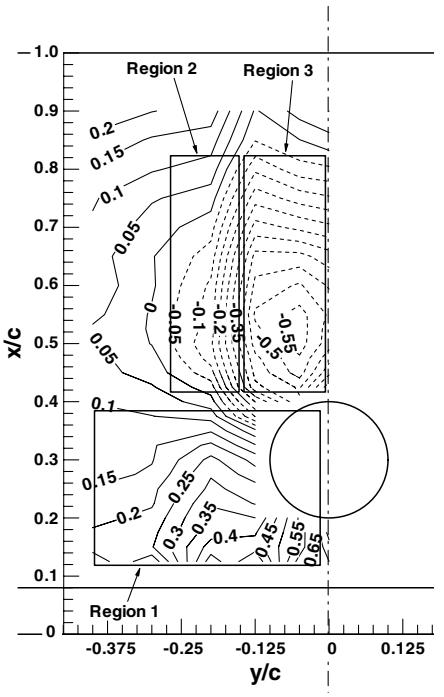

Fig. 8 Upper surface ΔC_P contours for the damaged model, at 12 deg incidence.

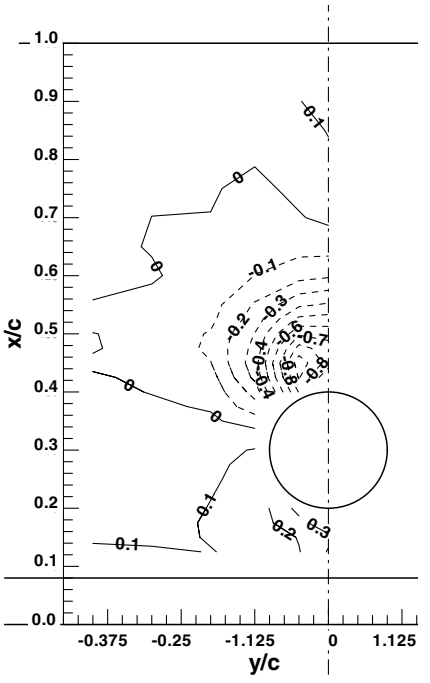

Fig. 9 Upper surface ΔC_P contours for the damaged model, at 8 deg incidence.

In this case, the positive C_p region can be seen to extend beyond the forward edge and over the front part of the damage hole. This, as seen in the flow visualization, is because the jet flow is confined to the rear part of the damage hole. Consequently, the region immediately upstream of the jet flow, which in this case incorporates the front portion of the damage hole, is subjected to a retardation of the oncoming freestream flow and hence positive induced C_p. The positive ΔC_p contours increase in magnitude closer to the jet, as the deceleration of the freestream flow becomes greater. The greatest positive C_p's are located toward the centerline of the damage hole, where the blockage effect of the exiting jet is greatest.

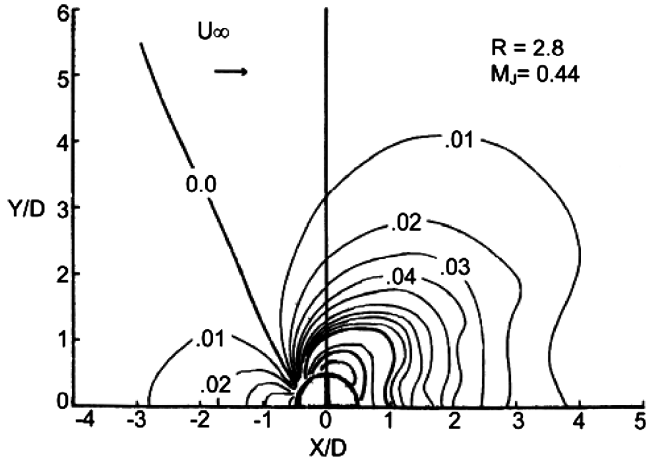

Fig. 10 Contours of constant C_P for a jet-in-crossflow [17].

Because the jet exits from the rear of the damage, the second region identified above (i.e., flow accelerating around the jet) is confined to the region behind the hole. The negative ΔC_p contours behind the damage hole can be seen to extend in a spanwise direction up to approximately 1.5 hole diameters from the centerline lending some evidence toward the width of the jet.

The third region from "jets in cross flow" is the distortion of the negative C_p contours toward the trailing edge immediately behind the damage, reflecting the close proximity of the deflected jet. The region of negative induced pressure behind the hole corresponds to the wake region of the jet, where reverse flow and entrainment occurs.

The three regions are also identifiable at 8 deg (Fig. 9), although as anticipated with a weak jet, they are significantly reduced in extent. The relatively low values of the positive ΔC_p contours forward of the hole confirm that the jet is confined to the rear of the damage.

Velocity Measurements in the Strong Jet

Plots of the velocity vectors in the x–z and x–y planes are shown for the strong jet at 12 deg in Figs. 11 and 12, respectively. These figures show contour plots of U_{true}, measured by the five hole probe. U_{true} has not been corrected for wind tunnel constraints. Velocity vectors are shown to give an indication on flow angularity. It should be noted that to avoid possible measurements errors due to surface proximity, velocity readings were not taken closer than 5 mm ($0.025c$) to the model surface. In addition, for vector measurements in the vicinity of the jet exit, the five hole probe was orientated along the z axis.

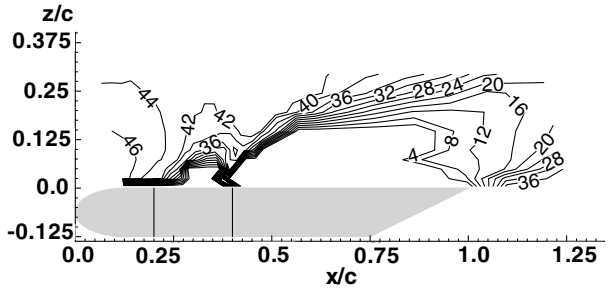

a)Velocity contours

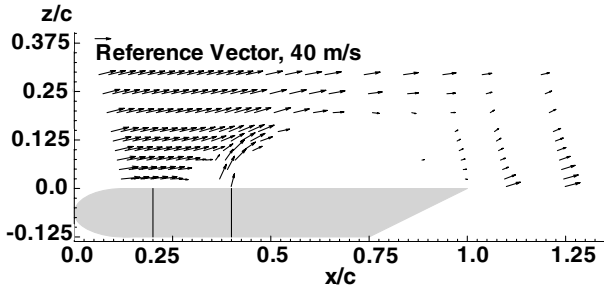

b) Velocity vectors

Fig. 11 Velocities in x–z plane of flat plate at 12 deg incidence.

In Fig. 11 the jet flow can be clearly seen penetrating into the freestream flow. However, the jet does not completely fill the damage hole and is confined to the rearmost portion, which confirms the observations of both the flow visualization and static pressure studies. The jet begins to bend over as soon as it exits the damage hole, but has enough momentum to penetrate approximately 1 hole diameter ($0.2c$) into the freestream before it is fully bent over. The precise size and shape of the jet is ambiguous, as the exact boundary between the jet and the freestream flow is difficult to distinguish. The magnitude of the velocity vectors reduces toward the trailing edge, indicating that the jet has begun to dissipate.

In both Figs. 11 and 12 two regions without velocity contours or vectors are apparent, upstream and downstream of the jet exit. These "zero-data" regions represent a "hole" in the data, where the local flow angles were outside the calibration of the five hole probe.

The smaller region immediately upstream of the jet exit is due to the oncoming flow bending around and also being entrained into the jet. The much larger zero-data region is downstream of the hole (and underneath the jet) and extends right up to the trailing edge. As the five hole probe has not measured any velocity vectors within this region, it can be concluded that all these vectors are either highly yawed or pitched, or both, so that they are beyond the calibration limits of the probe. Such extreme pitch and/or yaw angles can be explained with reference to previous jets in cross flow studies [20–24], where it has been established that there is a pair of contrarotating bound vortices attached to the underside of the jet. These vortices act to entrain the surrounding freestream flow toward the centerline and into the wake region. Evidence of this is given by the vectors along the edge of the reverse flow region, which can be seen to flow inwards toward the centerline (Figs. 12a–12c). As seen in the flow visualization, once the flow entered this region, it would naturally flow upstream (i.e., reverse flow) toward the damage hole before becoming entrained by the jet and flowing downstream with it. Thus, the length and height of this second zero-data region is indicative of the penetration of the jet. If the jet had attached to the surface or if it had dissipated, the reverse flow region itself would disappear.

Figure 12a, shows that the influence of the damage is fairly localized and from about 1 hole diameter ($0.2c$) away from the centerline has little influence on the flow toward the edge of the airfoil. In this region, the flow passes straight over the surface with negligible angularity. The only difference is that it accelerated from the undamaged case. This is expected, as the blockage effect caused by the jet and its wake would naturally cause the surrounding flow to accelerate. In this figure the two zero-data regions are joined. Comparison with the flow visualization (Fig. 6) indicates that this is in the vicinity of the contrarotating vortices and the forward edge of the jet.

Further away from the surface (Fig. 12b), the two zero-data regions separate and the aft zero-data region (reverse flow region) can be seen to reduce in size while simultaneously moving away from the rear edge of the damage hole. As this reverse flow region can only exist behind and underneath the jet (i.e., in its wake), its reduction in size and movement away from the hole edge shows the gradual bending of the jet by the freestream flow.

At a distance of approximately $0.1c$ away from the surface the first zero-data region (i.e., within the hole, upstream of the jet) has completely disappeared (Fig. 12c). At this distance the jet is heavily bent over, and consequently the oncoming flow bends around the jet gradually, resulting in much lower flow angles that fall within the calibration of the probe. The slightly yawed vectors just before the reverse flow region are evidence of the gradual bending of the oncoming flow.

Further away, at approximately $0.2c$ from the surface (Fig. 12d), the reverse flow region has disappeared, which indicates that the jet has been completely bent over by the freestream, and has begun to

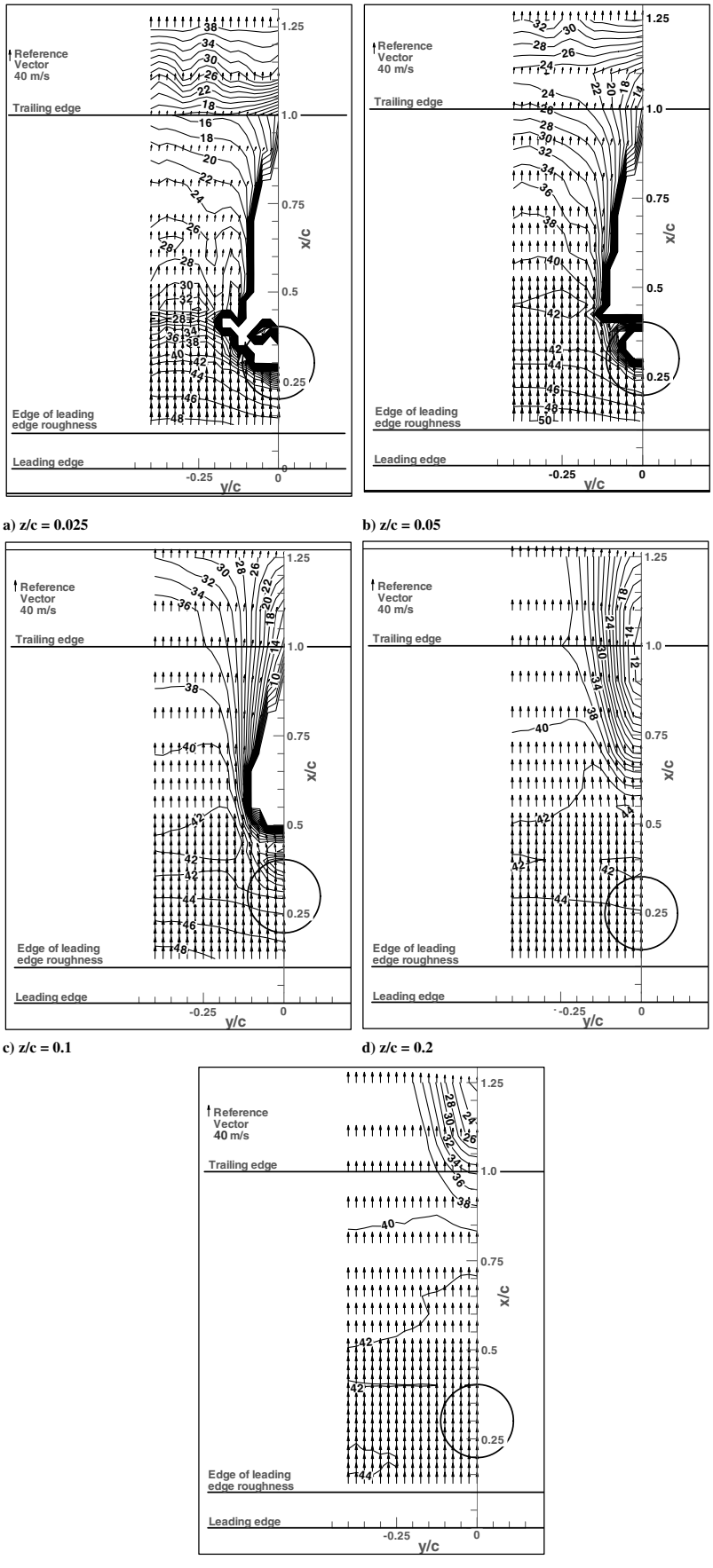

Fig. 12 ***x–y*** **data plots of** ***u–v*** **velocity vectors and** U_{true} **velocity contours, at various** z/c **from the aerofoil surface. Incidence = 1 deg.**

dissipate. At approximately $0.3c$ from the surface (Fig. 12e), the only evidence of the jet is the area of diminished velocity just aft of the trailing edge. At this distance, the flow resembles that of an undamaged model.

The jet-to-freestream velocity ratio for this angle of attack depends largely on the definition of the jet velocity, which is a difficult task as the lack of data in the exit plane prevents the clear identification of the jet boundary. The problem is compounded by the fact that the jet does not completely fill the damage hole at the exit plane, and is limited to the rearmost portion of the hole, giving it a highly irregular shape. Normally in jets-in-crossflow investigations, the jet fills out the entire hole and is not limited to part of the hole as found here. Also, in almost all jets-in-crossflow investigations, the jet has a flat velocity profile (i.e., the velocity at the edge of the jet is close to the velocity at the center of the jet). In such cases, the jet velocity can be easily defined by taking the average velocity across the exit plane. Other researchers [20,21,23,25] have used different definitions of the velocity ratio to counteract anomalies, such as when the difference between the center and edge velocities become significant. A common derivative of the velocity ratio in such cases is to calculate the jet-to-freestream momentum flux ratio. However, even this method requires an exact definition of the jet boundary. Nevertheless, approximate velocity ratios can be determined by taking an average of the U_{true} velocity vectors identified as being part of the through-hole jet in Fig. 12a. Using this method, R is 0.99. Andreopoulos [22] concluded that for jets in crossflow, a weak jet is present up until an R of about 0.5, and for R greater than 0.5 a strong jet flow is found. According to this definition, the current experiment would be classified as a strong jet. However, as already discussed the current experiment appears to be a transitional rather than a completely strong jet. It has to be noted that the limited data set available to calculate R may introduce some errors in the calculated value.

Velocity Measurements for the Weak Jet

Flow visualization showed that when the angle of attack was reduced to 8 deg there was a distinct change in the flow structure and a weak jet was formed. The velocity measurements shown in Fig. 13, illustrate this change of flow structure. Compared with the strong jet in Fig. 11, the penetration of the jet into the freestream is much less, and in fact, the jet is almost completely bent over as soon as it leaves the damage hole. Consequently, the reverse flow region in the wake of the jet is also significantly smaller. Once again there is a lack of data immediately in front of the jet, which is due to the oncoming flow bending laterally around the exiting jet. At this incidence this region is much smaller than previously, a consequence of the smaller and weaker jet. The jet also appears to dissipate into the freestream faster then the previous case. Although the flow features at this incidence suggest weak jet behavior, the calculated velocity ratio for this case is, surprisingly, 1.08. This is an unexpected result as it is greater than the velocity ratio calculated for the strong jet case. Based on Andreopoulos's criteria, a strong jet would be expected with this value of R. Although errors in R may have been introduced by the limited data available, it still provides an indication of the general magnitudes of the velocity ratios and, more important, a measure of their difference. Consequently, it can be concluded with some certainty that the velocity ratios at both angles of attack are similar. This leads on to two very important issues. First, the use of R from jets-in-crossflow studies is inappropriate to determine battle damage jet transition. Second, two similar velocity ratios have been seen to produce two different flow mechanisms. This contradiction is probably indicative of the inadequacy of defining the flow structure based merely on a velocity ratio. The flow structure is likely to be more dependent on the momentum ratio and also on the injection angle of the jet. The jet exit areas have been approximately determined to be 125 mm^2 for the strong jet (at 12 deg) and 75 mm^2 for the weak jet (at 8 deg). Dependency on the momentum ratio is suggested because, although the average jet velocity is similar for both angles of attack, the jet exits from a greater area of the hole at 12 deg than at 8 deg. Defining the momentum ratio at the ratio of the momentum of the jet divided by the momentum of the freestream flow through the wind tunnel working section resulted in a value of $M_R = 5.9 \times 10^{-4}$ for an incidence of 12 deg and $M_R = 3.8 \times 10^{-5}$ for 8 deg. The values are small because of the large size of the working section area compared with the jet area, but they do suggest that momentum ratio may be a better indication of jet transition.

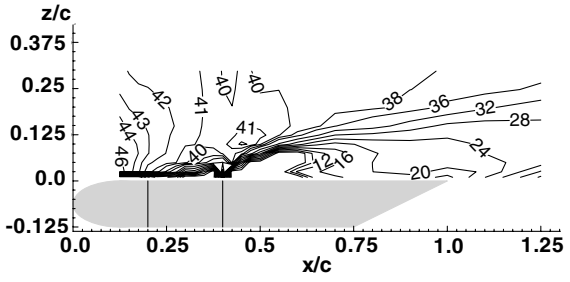

a) Velocity contours

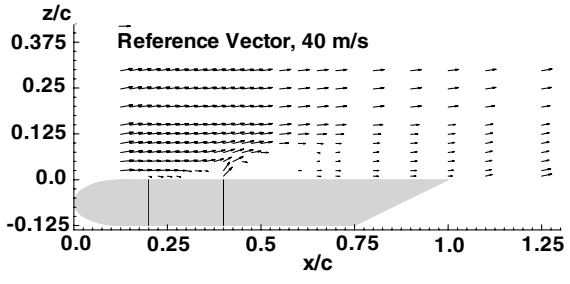

b) Velocity vectors

Fig. 13 Velocity vectors in x–z plane of flat plate at 8 deg incidence.

Noncircular Holes

Figure 14 shows the flow visualization for the star damage at 2 deg incidence. Primary (laminar) separation occurs upstream of the damage, and a horseshoe vortex forms that cuts through the airfoil's laminar separation bubble. Closer inspection of the front half of the damage reveals multiple flow paths where fluid is entrained from the damage into the horseshoe vortex. Three separate small jets exit from the rear of the damage. Two small vortices behind the rearmost apex signify one jet, and a small vortex behind each of the aft side apexes indicate that jets are also located here. Despite the multiple jets, the overall flow through the damage can be categorized as a weak jet. There was concern that the flow visualization at low incidences may have been significantly affected by the presence of the laminar separation bubble. To force boundary layer transition and remove the bubble, a 5 mm strip of 400 grit wet and dry abrasive sheet was

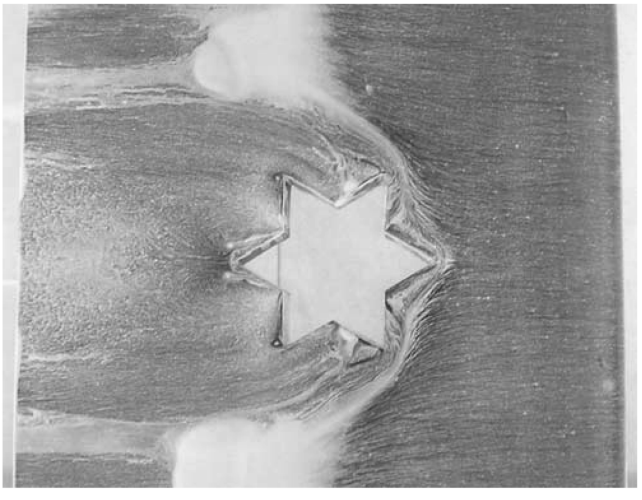

Fig. 14 Flow visualization for star damage at 2 deg incidence.

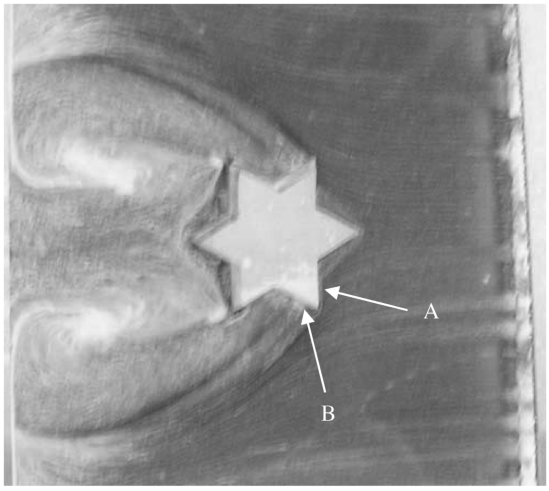

Fig. 15 Flow visualization for star damage at 8 deg incidence.

attached 10 mm behind the leading edge along the entire span of each model. The size and location of the damage jets, and the structure of the flow downstream of the damage was similar for both natural and forced transition, and it was concluded that the presence of the laminar separation bubble had no discernible effects on the flow through the damage.

At 4 deg incidence the damage jet flow had become transitional, and at 6 deg, strong jet flow was fully established. Figure 15 is the flow visualization for the star shaped damage at 8 deg incidence. The laminar separation bubble is now located at the leading edge of the model, and the primary separation due to damage occurs at the forward apex of the damage. However, the primary separation is deflected by the side apexes of the star (A). Secondary separation occurs from the side of the damage (B), and the resulting horseshoe vortex continues after the damage and is entrained into the large vortices. These two large vortices entrain flow from the underside of the model and carry it toward the damage. Upon meeting the damage jet this reverse flow separates and is entrained into the jet. The separation line is clearly modified by the presence of the rearmost apex, and the three separate jets identified at 2 deg have now effectively combined into a single jet. The width of the jet is indicated by the two small vortices behind the two rear side apexes of the star.

The flow visualization results indicated an increasing jet strength with incidence, and this would be anticipated to result in increased loss of lift coefficient, increased drag coefficient, and more negative pitching moment coefficient increments. These trends can be seen in Figs. 16–18, which show the increments plotted against incidence. By way of comparison, the results from Irwin [12] for the 20% chord circular damage are also shown. Of the four damage sizes tested by Irwin, in terms of damage area, this is the closest to the star shape.

From Fig. 16, the trends for the star damage are similar to those of the circle with increasing incidence resulting in an increased loss of lift. At extreme negative incidences the direction of the jet flow is reversed, resulting in the positive lift increments. Close to both negative and positive stall there is some uncertainty about the accuracy of the results, because a large extent of separated flow make the application of wind tunnel corrections difficult, and these results must be treated with caution. Although the trends of the star shape are similar to the circle, the results appear to be more "wavy." The uncertainties in the measurements make it difficult to analyze trends. However, it is worth noting that between 0 and 8 deg the flow through the damage showed significant differences for the two damage shapes. For the circle, transition from weak to strong jet occurred between 0 and 2 deg, whereas transition did not occur for the star until 6 deg. Compared with weak jets, strong jets are known to be more extensive and cause greater lift loss, and may well account for some of the "waviness."

Figure 17 shows drag coefficient increments against incidence for the star shape along with the circle results from Irwin. Above −4 deg, increasing incidence resulted in increased drag coefficient

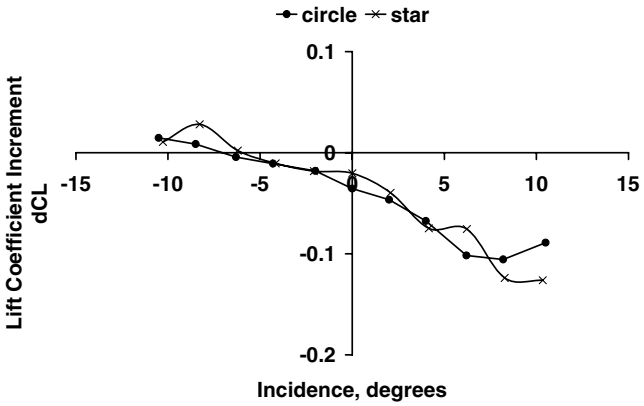

Fig. 16 Lift increments for NACA 64_1–412 airfoil.

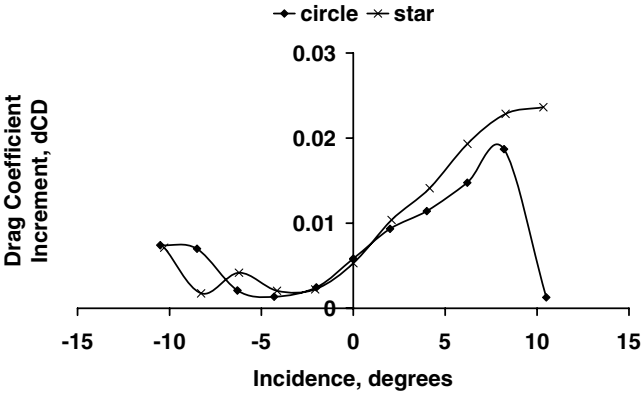

Fig. 17 Drag coefficient increments for NACA 64_1–412 airfoil.

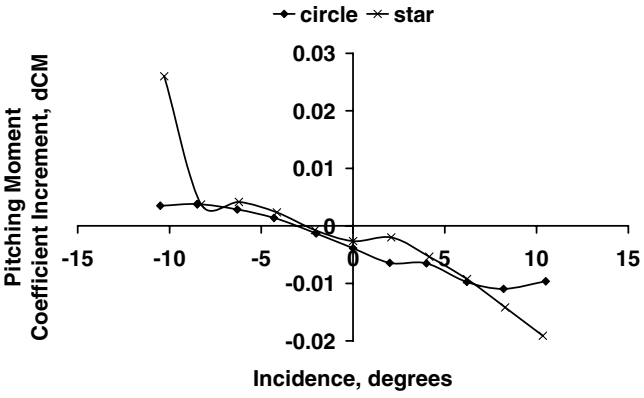

Fig. 18 Pitching moment coefficient increments for NACA 64_1–412 airfoil.

increments. The star and circle remain close to each other until 2 deg incidence, and with the quoted uncertainty cannot be distinguished from each other. At 2 deg incidence the circle damage had undergone transition to a strong jet, and interestingly started to produce significantly lower drag increments than the star. At −4 deg and below, the flow through the damage was reversed and its strength increased as incidence was reduced. As a result, drag increments generally increased.

Increments of pitching moment coefficient against incidence are shown in Fig. 18. The trend is for increased incidence to result in more negative increments. The star and circle produced similar increments to each other throughout most of the negative incidence range, and it should be noted that the uncertainty in both sets of measurements makes them difficult to separate. However, differences are apparent once transition to strong jet flow occurs for the circle (i.e., between 0 and 2 deg).

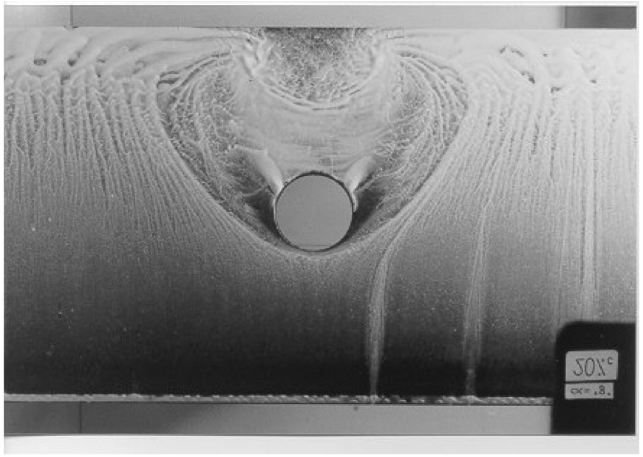

Fig. 19 Flow visualization for 20%c circle damage.

Despite the potential complexity of the flow, visualization showed that flow through the star damage could be categorized as weak, transitional, or strong jet, with the flow characteristics broadly similar to those identified by Irwin. Figure 19 has been provided by Irwin and is from the same body of work as [11]. It shows the 20% chord circle damage at 8 deg incidence. The strong jet exits from the rear of the hole, as is evident from the two small vortices. The distance between the two small vortices indicates that the jet width is less than the hole diameter. This implies that the jet for the circle is narrower than for the star at the same incidence (Fig. 15). However, apart from the jet width, there are significant similarities between the two flows. In terms of increments the only significant differences between the star and the circle are for drag and pitching moment, particularly at higher incidences. In terms of flow behavior, the circle is a reasonable approximation to the more complicated star shape, particularly when strong jet flows are present.

For the star it has been observed that the jet exits from the rear part of the hole. The hole geometry in the rear part of the damage determines the width of the jet, and the selection of a representative width is likely to be an important consideration when simulating battle damage. Increasing the circle diameter would probably improve the agreement, because Irwin showed that increasing circle diameter increased the size of the jet.

Conclusions

Reducing the camber of an airfoil weakens the strength and extent of the jet flow through battle damage, and delays the onset of transition from weak to strong jet flow. The reduction in jet strength reduces the size of drag and lift increments associated with battle damage.

On the upper surface of a flat plate airfoil with simulated battle damage, regions of static pressure coefficient changes induced by the damage flow are similar to those for jets in crossflow experiments. However, flow measurements on the damaged airfoil showed distinct differences from jets in crossflow because both weak and transitional strong jets exited from the rear of the damage hole and had nonuniform velocity profiles in the exit plane of the damage. For both jets, the jet-to-freestream velocity ratio was close to 1. This is significantly higher than the value of 0.5 frequently used to determine transition for jets in cross flows, and suggests that the criteria is inappropriate for battle damage studies. For battle damage it was noted that the use of a criteria based on momentum was likely to be more appropriate.

For star shaped battle damage, despite the presence of multiple sharp edges, the overall characteristics of the through flow can be categorized as weak, transitional, or strong jet. The main features of these flows are identical to those for circular damage.

For star damage, increasing incidence generally resulted in greater lift loss, higher drag, and more negative pitching moment. These changes in aerodynamic coefficients were similar in value to those previously reported for circular damage of a similar area to the star.

Finally, it can be concluded that circular holes are a reasonable representation of battle damage provided the diameter is close to the maximum width of the damage being simulated.

Acknowledgments

The authors are grateful for the help and assistance of Peter Stinchcombe and Rob Hunter in manufacturing the models. The help of Pat Griffin and Goff Tearle in producing some of the figures is also gratefully acknowledged. Thanks are also extended to Andrew Irwin who provided the photograph for Fig. 19.

References

[1] Scott, D. S., and Westkaemper, J. C., "The Influences of Ballistic Damage on the Aeroelastic Characteristics of Lifting Surfaces," University of Texas at Austin, Air Force Office of Scientific Research TR-80-0220, 1979.

[2] Hayes, C., "Effects of Simulated Wing Damage on the Aerodynamic Characteristics of a Swept-Wing Aeroplane Model," NASA TMX-1550, 1968.

[3] Lamb, M., "Effects of Simulated Damage on Stability and Control Characteristics of a Fixed-Wing Twin-Vertical-Tail Fighter Model at Mach Numbers from 2.50 to 4.63," NASA TMX-2815, 1973.

[4] Spearman, M. L., "Wind Tunnel Studies of the Effects of Simulated Damage on the Aerodynamic Characteristics of Aeroplanes and Missiles," NASA TM-84588, 1982.

[5] Betzina, M. D., and Brown, D. H., "Aerodynamic Characteristics of an A-4B Aircraft with Simulated and Actual Gunfire Damage to One Wing," NASA TMX-73119, 1976.

[6] Stearman, R. O., and Chang, J. H., "The Effects of Warhead Induced Damage on the Aeroelastic Characteristics of Lifting Surfaces: Aeroelastic Effects," University of Texas at Austin, Air Force Office of Scientific Research TR-80-1039, Vol. 1, 1980.

[7] Leishman, J. G., "Aerodynamic Characteristics of a Helicopter Rotor Airfoil as Affected by Simulated Ballistic Damage," University of Maryland AD-A269 206, 1993.

[8] Robinson, K. W., and Leishman, J. G., "Effects of Ballistic Damage on the Aerodynamics of Helicopter Rotor Airfoils," *Journal of Aircraft*, Vol. 33, No. 5, 1998, pp. 695–703.

[9] Irwin, A. J., Render, P. M., McGuirk, J. J., Probert, B., and Alonze, P. M., "Initial Investigations into the Aerodynamic Properties of a Battle Damaged Wing," AIAA Paper 95-1845, June 1995.

[10] Irwin, A. J., and Render, P. M., "The Influence of Internal Structure on the Aerodynamic Characteristics of Battle-Damaged Wings," AIAA Paper 96-2395, June 1996.

[11] Irwin, A. J., and Render, P. M., "The Influence of Mid-Chord Battle Damage on the Aerodynamic Characteristics of Two-Dimensional Wings," *The Aeronautical Journal*, Vol. 104, No. 1033, 2000, pp. 153–161.

[12] Irwin, A. J., "Investigation into the Aerodynamic Effects of Battle Damage," Ph.D. Thesis, Loughborough University, U.K., 1999.

[13] Mi, J., Nathan, G. J., and Luxton, R. E., "Centreline Mixing Characteristic of Jets from Nine Different Shaped Nozzles," *Experiments in Fluids*, Vol. 28, No. 1, 2000, pp. 93–94.

[14] Mani, M., and Render, P. M., "Experimental Investigation into the Aerodynamic Effects of Airfoils with Triangular and Star Shaped Through Damage," AIAA Paper 2005-4978, June 2005.

[15] Garner, H. C., "Subsonic Wind Tunnel Wall Corrections," AGARDograph 109, 1966.

[16] Loftin, L. K., and Smith, H. A., "Aerodynamic Characteristics of 15 NACA Airfoil Sections at Seven Reynolds Numbers from 0.7×10^6 to 9.0×10^6," NACA TN 1945, 1949.

[17] Fearn, R. L., and Weston, R. P., "Induced Pressure Distribution of a Jet in a Crossflow," NASA TN D-7916, 1975.

[18] Wooler, P. T., "On the Flow Past a Circular Jet Exhausting at Right Angles From a Flat Plate or Wing,". *Journal of the Royal Aeronautical Society*, Vol. 71, Mar. 1966, pp. 216–218.

[19] Vogler, R. D., "Surface Pressure Distributions Induced on a Flat Plate by a Cold Air Jet Issuing Perpendicularly from the Plate and Normal to a Low Speed Freestream Flow," NASA TN-D-1629, Jan. 1963.

[20] Kamotani, Y., and Greber, I., "Experiments on a Turbulent Jet in a Crossflow," *AIAA Journal*, Vol. 10, No. 11, 1972, pp. 1425–1429.

[21] McMahon, H. M., and Antani, D. L., "An Experimental Study of a Jet Issuing from a Lifting Wing," *Journal of Aircraft*, Vol. 16, No. 4, 1979, pp. 275–281.

[22] Andreopoulos, J., and Rodi, W., "Experimental Investigation of Jets in a Crossflow," *Journal of Fluid Mechanics*, Vol. 138, Jan. 1984, pp. 93–127.

[23] Mikolowsky, W., and McMahon, H., "An Experimental Investigation of a Jet Issuing from a Wing in Crossflow," *Journal of Aircraft*, Vol. 10, No. 9, 1973, pp. 546–553.

[24] Fearn, R. L., and Weston, R. P., "Vorticity Associated with a Jet in a Crossflow," *AIAA Journal*, Vol. 12, No. 12, 1974, pp. 1661–1671.

[25] Rudinger, G., and Moon, L. F., "Laser-Doppler Measurements in a Subsonic Jet Injected into a Subsonic Crossflow," *Journal of Fluids Engineering*, Vol. 98, Sept. 1976, pp. 516–520.